Tidal stream power in the Pentland Firth – long-term variability, multiple constituents and capacity factor

Long-term available power predictions for the Pentland Firth

Thomas A.A. Adcock[a,1], Scott Draper[b], Guy T. Houlsby[a], Alistair G. L. Borthwick[c], Sena Serhadlıoğlu[a]

[a] *Department of Engineering Science, University of Oxford*
[b] *Centre for Offshore Foundation Systems, The University of Western Australia*
[c] *Institute of Energy Systems, The University of Edinburgh*

Abstract

The Pentland Firth, Scotland, is one of the World's prime locations for the eventual installation of large farms of tidal stream turbines. This paper seeks to improve the upper bound estimate of available power output obtained by Adcock *et al.* (2013) who used a depth-integrated numerical model of the region containing the Pentland Firth with the outer boundary forced solely by M_2 and S_2 tidal constituents. Herein, the analysis is extended to include six additional tidal constituents and the model run for 11.5 years, more than half of the 18.6 year lunar nodal cycle, to allow variations over this to be analysed analysed. The consequent increase in available power is estimated, and the variation in power output over an eleven-year period is examined. Although further power could theoretically be extracted from the additional six tidal constituents, this would require the tidal turbine farm to have such a low capacity factor that it would probably be economically unfeasible.

Keywords: Pentland Firth, Available power, Power potential, Capacity factor, 18.6 year lunal nodal cycle

1. Introduction

The Pentland Firth separates the northern mainland of Scotland from the Orkney Islands. The Firth effectively comprises a narrow strait linking the Atlantic Ocean to the North Sea, and carries tidal currents whose speed often exceeds 3 m/s. Consequently, the Firth is widely regarded as one of the most important and promising sites for the deployment of arrays of tidal stream turbines. A good understanding of the tidal flow conditions and accurate assessment of the possible power output of small turbine arrays within the Firth remain open questions, due to a lack of detailed field measurements. However, Adcock *et al.* [1] made an approximate estimate of the upper limit on the available power that can be generated from the site using a depth-integrated numerical model of the tidal dynamics in the region. The model was forced solely by the dominant M_2 and S_2 tidal constituents. In the present paper we extend the analysis to consider a model forced by the eight largest tidal

Email address: thomas.adcock@eng.ox.ac.uk (Thomas A.A. Adcock)

constituents and examine the available power time history over a long time-frame. Whilst other studies of different sites (such as [2, 3]) have considered a full set of tidal constituents these models were only run for short time-spans and do not analyse the long-term variations in power analysed in this paper.

This paper has three main objectives. Firstly, we examine how the power varies with the nodal factor of the M_2 tidal constituent and how this changes the magnitude of the tidal stream resource from year-to-year. The second objective is to examine how much extra power is available to a tidal turbine farm in the Pentland Firth from the additional tidal constituents and to examine how this power varies with time. The final objective is to demonstrate certain key characteristics of tidal turbine farms, such as the effect on the capacity factor of using tidal turbines with a rated power large enough to extract all the available power.

2. Numerical model

The numerical model used in this paper is identical to that used by Adcock *et al.* [1] who provide a full discussion of the numerical scheme, its limitations, and its validation. A very brief description follows. The model is based on the depth-integrated shallow water equations commonly used for tidal flow simulation, which are solved using the discontinuous Galerkin version of ADCIRC [4, 5]. The model domain extends to the continental shelf to the west of the Pentland Firth and an approximately equal distance to the east. After calibration, the model predictions of water levels were found to be in excellent agreement with observed data across the domain. Care was taken to tune the bed friction coefficient within the model to obtain agreement with the limited field data available for currents within the Pentland Firth. Allowing for some discrepancies, the agreement between model predictions and field data was sufficiently close to give confidence that the primary features of the flow have been captured (see section 3 in reference [1]).

The effect of a row of tidal turbines is represented using a line-discontinuity within the model to simulate the head-loss across the turbine following the approach proposed by Draper *et al.* [6] which has been compared to physical experiments in [7]. The head loss is calculated using linear momentum actuator disc theory following Houlsby *et al.* [8] and incorporated within the numerical code as a momentum sink [9]. The model has been applied to the analysis of other sites in [10, 11]. The model accounts for both the extracted power (the total removed from the flow) and the available power (the inviscid upper limit of shaft power of the tidal turbines). The present paper considers solely the available power. Following [1], we seek to investigate the upper bound for the amount of power which is available to tidal turbines in the Pentland Firth. Thus we neglect cut-in velocities, the rated power of the turbines, and any drag due to the support structure of the turbines.

3. Methodology

The aim of this paper is to extend the results of Adcock *et al.* [1] by examining the variation in available power over a much longer time frame using Adcock *et al.*'s model

forced with a more complete set of tidal constituents at the open outer boundary. Due to the computational demands of longer simulations investigation is restricted to two cases. One case considers three rows of turbines, with a blockage ratio of 0.4; the other considers a single row of turbines with a blockage ratio of 0.1. The turbines are placed in the fastest flows within the channels between South Ronaldsay and Swona, Swona and Stroma, and Stroma and the mainland. Figure 1 shows the location of the turbines. Thus the turbine fence extends across the entire width of the Pentland Firth. Blocking of different channels within the strait is considered in [12, 13].

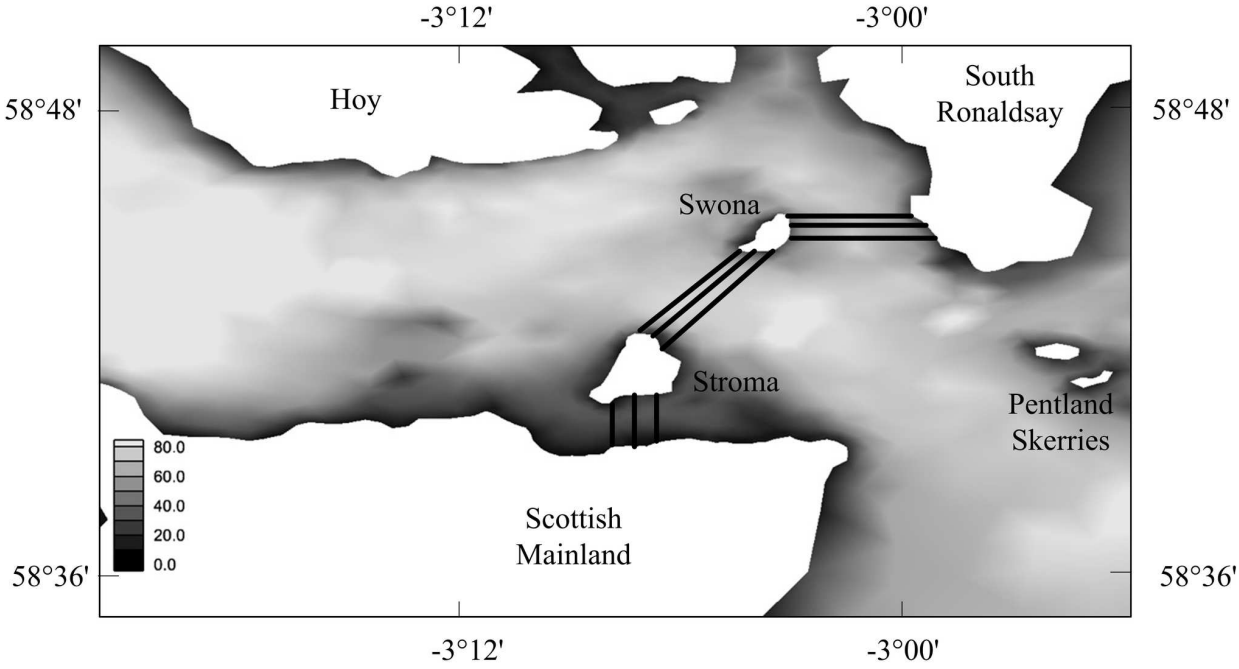

Figure 1: Map of the Pentland Firth area showing the locations of the three turbine fences used in this study. When one rows is simulated the turbine row is the furthest west/north or the rows shown. Bathymetry is shown in grey-scale with depths in m.

Following Vennell [14], Adcock *et al.* [1] discuss the need to 'tune' the wake velocity coefficient of the turbines to optimise the available power. In [1] the wake induction factor was varied over the spring/neap cycle noting that the dynamic balance of the channel varied between spring and neap tides (see also [15]). However, use of a time-dependent wake velocity coefficient led to minimal increase in the amount of available power, and so this was not implemented in the present work. Instead, the optimum constant wake velocity coefficients over a typical spring/neap cycle were found and used throughout both simulations. The wake velocity coefficients used were: 0.51 for three rows of high blockage turbines; and 0.34 for a single row of low blockage turbines.

At the open boundaries, the model was forced by 8 different tidal constituents: K_1, K_2, M_2, MU_2, N_2, NU_2, O_1 and S_2. All other constituents were extremely small at the

Tidal constituent	Magnitude of head difference(m)
M_2	1.36
S_2	0.55
N_2	0.30
K_2	0.12
MU_2	0.075
NU_2	0.053
O_1	0.049
K_1	0.045

Table 1: Magnitude of the head difference across the Pentland Firth for the eight tidal constituents considered in this study. The head difference is based on the difference between the water levels at 58.78°N 3.83°W and 58.64°N 2.80°W

open boundaries and had virtually no impact on the tidal dynamics in the Pentland Firth. To indicate the importance of each constituent on the tidal dynamics within the Firth, Table 1 lists the head difference across the Pentland Firth due to the different constituents, although it should be noted that there is always ambiguity about exactly where to take the measurements used to compute the head difference. The simulations presented here start on 1 February 2014 and extend for $\sim$ 11.5 years (4260 days) so as to reproduce more than half of the 18.6 year nodal cycle. For computational reasons, this period was split up into sixty day sections over which the nodal factor of each constituent was held constant. A model spin-up period of two days was implemented for each 60 day segment. When the individual sixty day simulations were combined together, there was virtually no mismatch between adjacent simulations.

4. Variations in power over the nodal tidal cycle

The angle between the plane of the Moon's orbit around the Earth, and the plane through the equator of the Earth varies, with a period of 18.6 years. This influences all the tidal constituents used in this model with the important exception of the S_2 constituent. The nodal tidal cycle is usually represented as a linear modulating factor in the calculation of tidal amplitudes. Thus for the M_2 constituent,

$$\eta_{M_2} = f_{M_2} \times a_{M_2} \cos\left(\omega_{M_2} t + g\right), \tag{1}$$

where η_{M_2} is the water level variation at the frequency of M_2, f_{M_2} is the nodal factor, a_{M_2} is the amplitude of the M_2 constituent, ω_{M_2} is the frequency of the M_2 tide and g its phase.

The dominant tidal constituent varies across the world [16]. At most candidate sites for tidal stream energy extraction the M_2 constituent dominates the tidal regime. Thus, the variations in power from year to year are going to be dominated by the value of the f_{M_2}. Figure 2 shows how the M_2 nodal factor varies over the time-span considered in this paper.

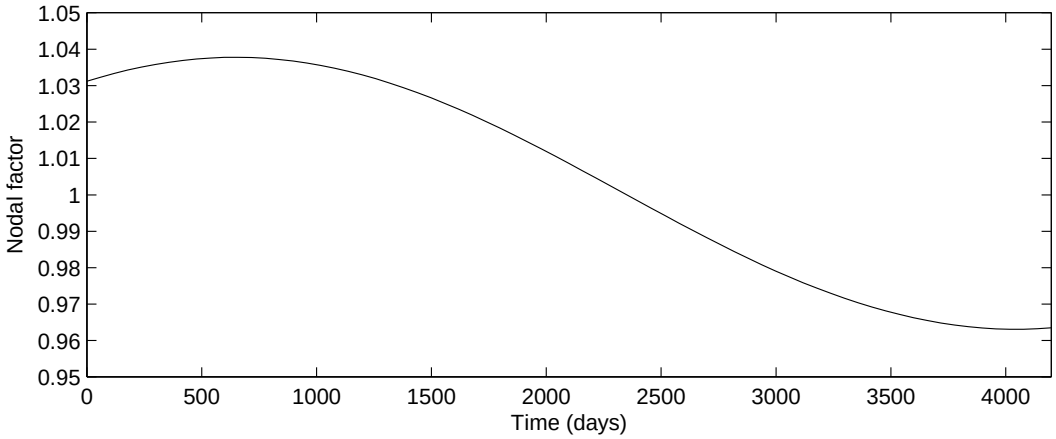

Figure 2: Variation in M_2 nodal factor over the analysis period. Zero time is at 1 February 2014.

In the open ocean, the amplitude of the M_2 water level is usually assumed to vary in proportion to the nodal factor as given in equation 1. If this proportional relationship is assumed to extend to fast flowing tidal currents then velocity will scale with nodal factor too, meaning power would scale with nodal factor cubed. However, in areas of shallow, fast flowing tidal currents proportionality cannot be assumed due to the non-linear nature of these flows (as noted by Parker *et al.* [17]). Numerical simulations are undertaken to analyse fully how the tidal stream resource of a site varies. As a preliminary investigation, the model is run with only the M_2 constituent but with the nodal factor varied. Figure 3 shows the variation in the mean available power predicted by the model for the varying nodal factors.

Figure 3 shows that the predicted available power increases monotonically with nodal factor over the range of values tested, but with a lower sensitivity to the nodal factor than would be predicted assuming a linear relationship between current and nodal factor. The variation in available power with nodal factor is smaller for larger-scale deployments of turbines (which introduce increased non-linear drag into the system). To examine the effect of nodal variations on the available power in the Pentland Firth when the model is forced with eight tidal constituents, Figure 4 shows the mean available power in each calendar year from 2015 to 2023 inclusive. The duration of the simulations includes nodal factors over the full range of values. The mean available power in 2023 (when the nodal factor is a minimum) is 88% of that in 2015 (when the nodal factor is a maximum) for 3 rows/0.4 blockage and 87% for 1 row/0.1 blockage. These variations are therefore important and should be taken into account in resource assessments (as also noted by Stock-Williams et al. [18]).

5. Mean available power

Table 2 presents the mean power output from the model forced solely by the M_2 tide, the M_2 and S_2 tide, and the eight largest tidal constituents over a period of 9.3 years starting

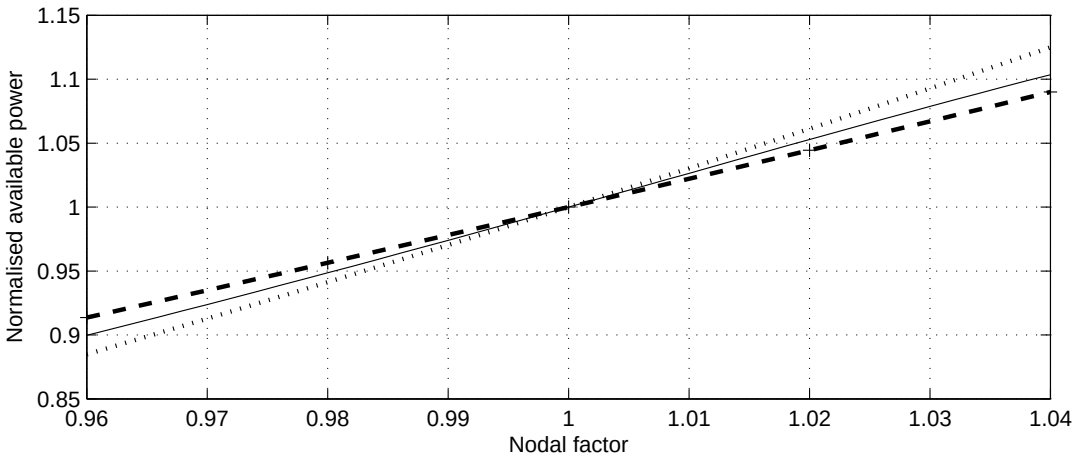

Figure 3: Variation in mean available power for the Pentland Firth with model forced only with the M_2 tidal constituent. Available power normalised by available power with nodal factor of one. Thick dashed line – 3 rows/0.4 blockage; thin line – 1 row/0.1 blockage; thick dotted line – cubic relationship between power and nodal factor.

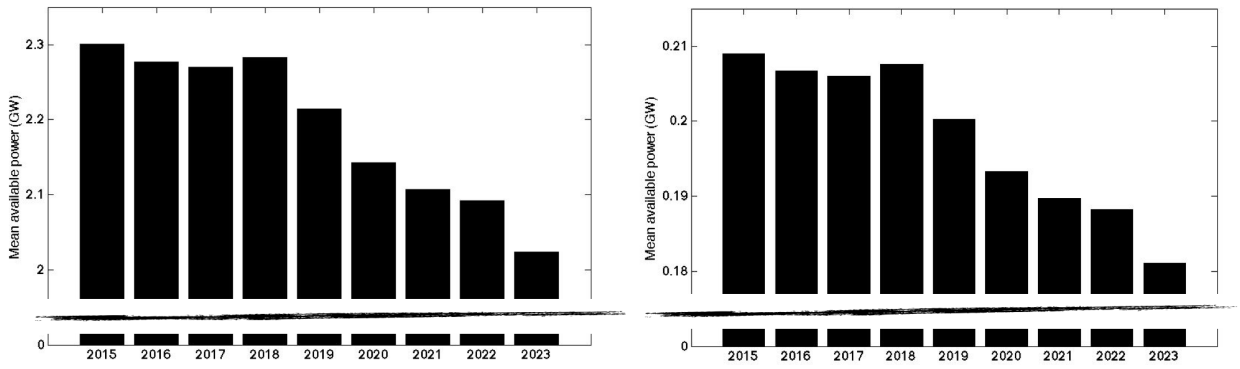

Figure 4: Mean annual available power over the calendar years 2015 to 2023. Left – 3 rows/0.4 blockage; right – 1 row/0.1 blockage.

	M_2	M_2 and S_2	Eight constituents
3 rows, high blockage	1.74	2.05	2.16
1 row, low blockage	0.150	0.183	0.195

Table 2: Mean available power predictions from the model when forced by different tidal constituents. Power in GW

when the M_2 nodal factor is a maximum and finishing when it is a minimum (see Figure 2).

When more tidal constituents are used to drive the model, the estimate of available power increases. There is a proportionately greater increase in available power as further constituents are added for the single row/low blockage case than for the highly blocked case. This is to be expected, and is discussed at length by Adcock & Draper [15]. Briefly, the reason is that the thrust the turbines apply to the flow is much more significant in the highly blocked case, and this reduces the strength of the faster currents more than it reduces the slower currents.

6. Variation in power output

Tidal power is intermittent, with no power generated at slack water and large values of power being available for short periods when the flow is strongest. In practice, it is unlikely to be feasible to extract all the peaks in available power. (This is discussed further in section 6.2). As an example of the variation in available power over a typical month, Figure 5 shows the power output over February 2014.

For both cases considered in Figure 5 there is a significant difference between the power produced at spring tide (about 1 day after the start of the analysis) and neap tide (about 7 days later). The relative difference is larger for the single row of turbines with small blockage (consistent with [1]). There is also greater relative variation in the daily power record for the smaller deployment of turbines.

6.1. Variation between different spring/neap cycles

The dominant tidal constituents in the Pentland Firth are the M_2 and S_2 components which establish the regular fortnightly spring/neap tidal cycle which is evident in Figure 5. This regular oscillation is perturbed by the remaining tidal constituents. To examine this perturbation over time it is convenient to remove the variation in power over time-scales shorter than tens of hours. We do this by low-pass filtering the data. Figure 6 shows the low-pass filtered time series for just over three years starting 1 February 2014. In Figure 6 each peak is a spring tide and each trough a neap tide. The dominant oscillation in the amount of power available at spring or neap tide is due to the interaction with the N_2 constituent. Components smaller than N_2 have almost no impact at this scale.

6.2. Rated power and capacity factor

In practice the operating characteristics of tidal turbines will differ very significantly from the actuator disc model used in this paper. For example, the power generated by

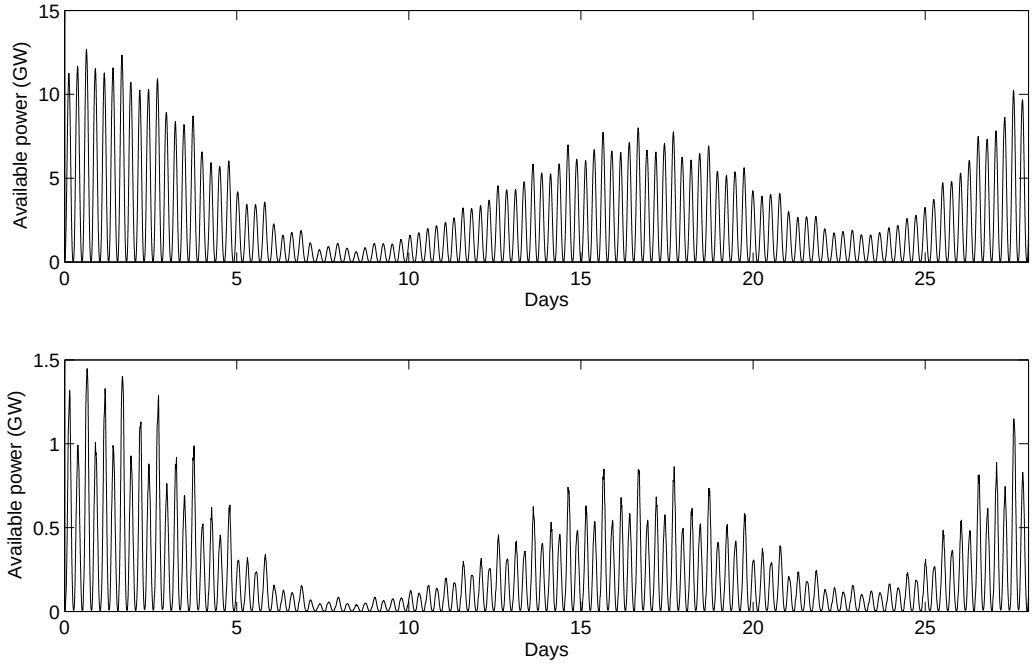

Figure 5: Available power over the month of February 2014. Top: 3 rows/0.4 blockage. Bottom: 1 row/0.1 blockage.

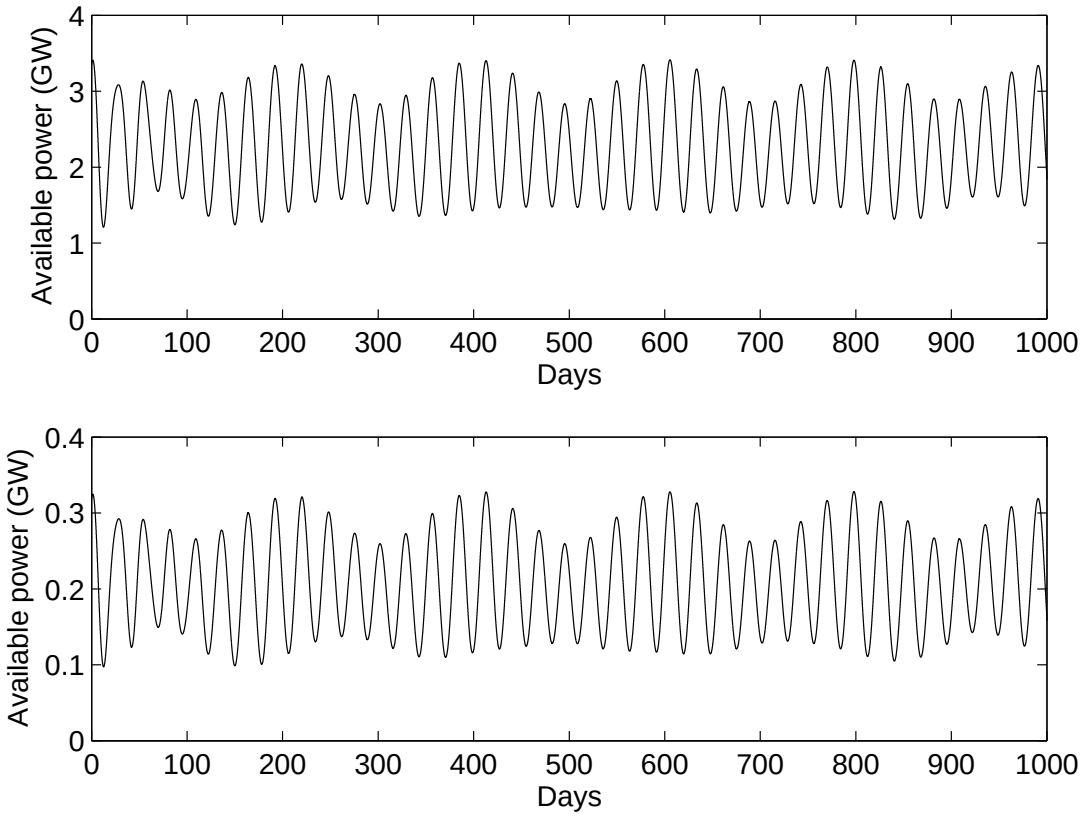

Figure 6: Time series filtered to remove the daily tidal cycle. Top 3 rows/0.4 blockage. Bottom 1 row/0.1 blockage.

tidal turbines will be 'capped' by the capacity of the generators employed, and so they will not be able to capture all the power in the peaks shown in Figure 5. Such power capping will mainly be implemented to reduce the required capacity of the generator and cabling required, to reduce the loads on the turbine, and to reduce the gearing demands.

The most likely way in which power capping will be implemented will be to run the turbine at a lower tip speed ratio for the fastest flows to change the power coefficient and so keep the power produced constant. This will, in turn, reduce the thrust coefficient which in turn will cause a change in the channel dynamics. An alternative strategy would be to increase the tip speed ratio which would imply an increased thrust coefficient. A further consideration is that even if the thrust coefficient of the turbine reduces, there will also be a substantial drag from the support structure which will not be significantly altered by power capping [19]. All these factors will feed into the channel dynamics and will have a feedback on the current in the channel and therefore the power production. Having a varying turbine drag can produce complicated results for highly blocked channels with the power able to go up or down depending on the strategy used [20, 21]. Given that the detailed turbine characteristics are not known we have made the crude assumption that the thrust coefficient will take the same value whether or not there is any power capping. Numerical experiments using the simple channel model of [22] suggests that this approach is justified, with differences in mean power generation of less than 2% between the approach taken here and an approach that reduced the turbine thrust as power was capped. Further justification of this approach is that typically power capping will only occur for a relatively short section of the tidal cycle and the channel dynamics are dependent on the thrust over the whole cycle.

Figure 7 shows that much of the total available energy can still be captured even if the rated power of the generator is reduced substantially from that needed to extract the maximum instantaneous available power. For instance, for the less intense development, 90% of the available energy can be extracted by turbines with only 35% of the generation capacity that would be required to extract the final 10% of available energy. For this reason the upper bound of estimate of time-average power generation made by Adcock *et al.* [1] is unlikely to be exceeded in practice, even though more power is available from the additional tidal constituents.

For the different relative rated powers it is also possible to estimate a 'capacity factor' for the tidal turbine farm. This is defined as the mean power generated divided by the rated power of the tidal turbine farm. Figure 8 shows the variation in capacity factor for both the tidal farm layouts considered in this paper. This highlights the infeasibility of sizing the generators to exploit all the available power. Figure 8 also demonstrates an advantage of a large turbine farm over a smaller, in that the former has an inherently higher capacity factor.

The analysis presented in Figures 7 and 8 simply takes into account an upper limit for power capping. The matching of the generation capacity to the resource would also be affected by lower limits on available power, as most practical devices would not operate at all below a certain cut-in velocity, although mean power generation is likely to be insensitive to this value.

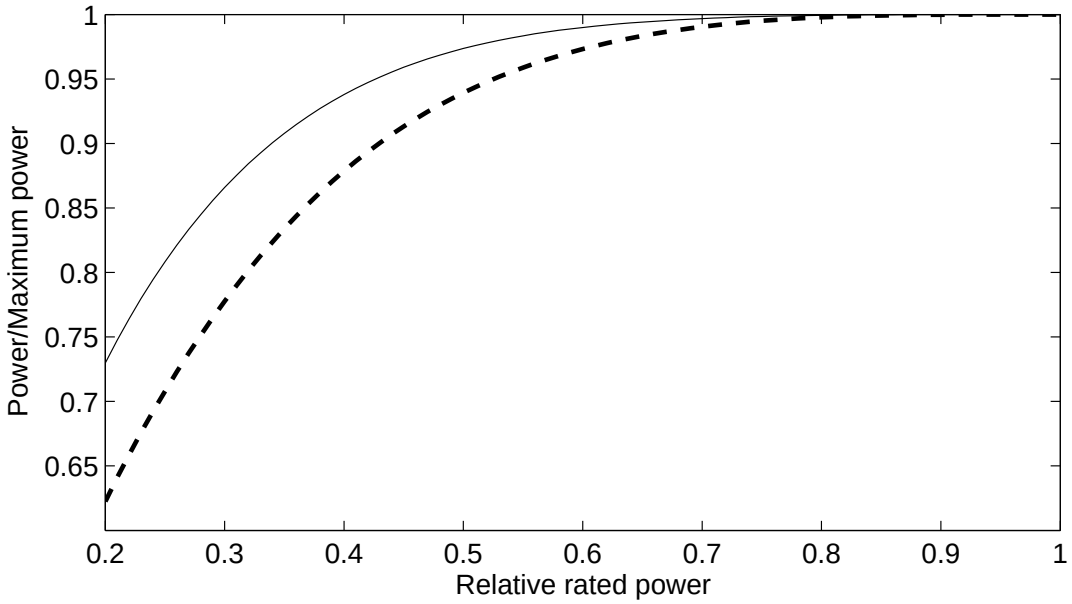

Figure 7: Long-term time averaged available power plotted against rated power of a turbine farm as a fraction of the rated power required for all the available power to be utilised. Thick dashed line – 3 rows/0.4 blockage; thin line – 1 row/0.1 blockage.

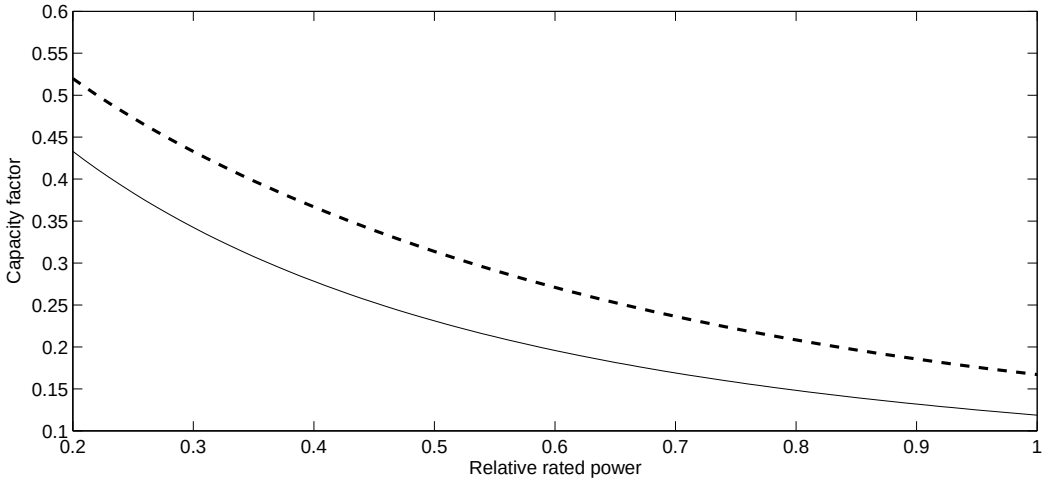

Figure 8: Capacity factor of the tidal turbine farm for different relative rated powers. Thick dashed line – 3 rows/0.4 blockage; thin line – 1 row/0.1 blockage.

7. Conclusions

This paper has extended the analysis of the tidal resource of the Pentland Firth given by Adcock *et al.* [1] to include a further six tidal constituents in addition to M_2 and S_2. Long time-series were simulated in order to examine the variation over the 18.6 year lunar nodal tidal cycle. The predictions show that the tidal power resource does vary over the nodal cycle, with the mean available power in 2023 being approximately 87% of the mean available power in 2015 for identical installations of turbines. Forcing the model with additional constituents (K_1, K_2, MU_2, N_2, NU_2 and O_1) in addition to M_2 and S_2 yields a small increase in the theoretical available power; for the two extreme cases considered herein the increase is $\sim 5\%$ for a very large tidal farm and $\sim 7\%$ for a small farm. But this increase coincides with larger extremes in instantaneous available power and is therefore unlikely to be realized in practice because the rated power (capacity factor) to remove all of the power associated with these extremes will be excessively high (low).

Acknowledgements

This work was commissioned and supported by the Energy Technologies Institute as part of the PerAWaT project. S.D. would like to acknowledge the support of the Lloyd's Register Foundation. Lloyd's Register Foundation invests in science, engineering and technology for public benefit, worldwide.

References

[1] T. A. A. Adcock, S. Draper, G. T. Houlsby, A. G. L. Borthwick, S. Serhadlıoğlu, The available power from tidal stream turbines in the Pentland Firth, Proc. R. Soc. A 469 (2157) (2013) 20130072. doi:10.1098/rspa.2013.0072.

[2] R. Carballo, G. Iglesias, A. Castro, Numerical model evaluation of tidal stream energy resources in the Ra de Muros (NW Spain), Renewable Energy 34 (6) (2009) 1517 – 1524. doi:http://dx.doi.org/10.1016/j.renene.2008.10.028.

[3] R. Ahmadian, R. Falconer, B. Bockelmann-Evans, Far-field modelling of the hydro-environmental impact of tidal stream turbines, Renewable Energy 38 (1) (2012) 107 – 116. doi:http://dx.doi.org/10.1016/j.renene.2011.07.005.

[4] E. J. Kubatko, J. J. Westerink, C. Dawson, hp Discontinuous Galerkin methods for advection dominated problems in shallow water flow, Computer Methods in Applied Mechanics and Engineering 196 (1-3) (2006) 437 – 451. doi:10.1016/j.cma.2006.05.002.
URL http://www.sciencedirect.com/science/article/B6V29-4M1CYTM-1/2/6c45c85d20d17690046881a795b0b0

[5] E. J. Kubatko, S. Bunya, C. Dawson, J. J. Westerink, C. Mirabito, A performance comparison of continuous and discontinuous finite element shallow water models, J. Sci. Comput. 40 (1-3) (2009) 315–339. doi:10.1007/s10915-009-9268-2.

[6] S. Draper, G. T. Houlsby, M. L. G. Oldfield, A. G. L. Borthwick, Modelling Tidal Energy Extraction in a Depth-Averaged Coastal Domain, IET Renewable Power Generation 4 (6) (2010) 545 – 554. doi:10.1049/iet-rpg.2009.0196.

[7] S. Draper, T. Stallard, P. Stansby, S. Way, T. Adcock, Laboratory scale experiments and preliminary modelling to investigate basin scale tidal stream energy extraction, in: 10th European Wave and Tidal Energy Conference (EWTEC), Aalborg, Denmark, 2013.

[8] G. T. Houlsby, S. Draper, M. Oldfield, Application of Linear Momentum Actuator Disc Theory to Open Channel Flow, Technical report 2296-08, University of Oxford (2008).

[9] S. Serhadlıoğlu, G. T. Houlsby, T. A. A. Adcock, S. Draper, A. G. L. Borthwick, Assessment of Tidal Stream Energy Resources in the UK Using a Discontinuous Galerkin Finite Element Scheme, in: FEF February 24-27 2013, San Diego, California, 2013.

[10] S. Serhadlıoğlu, T. A. Adcock, G. T. Houlsby, S. Draper, A. G. Borthwick, Tidal stream energy resource assessment of the Anglesey Skerries, International Journal of Marine Energy 34 (0) (2013) e98 – e111, special Issue Selected Papers - {EWTEC2013}. doi:http://dx.doi.org/10.1016/j.ijome.2013.11.014.

[11] T. A. A. Adcock, S. Draper, On the tidal stream resource of two headland sites in the English Channel: Portland Bill and Isle of Wight, in: 33rd International Conference on Ocean, Offshore and Arctic Engineering, 8 - 13 June, San Francisco, California, no. 23032, 2014.

[12] S. Draper, T. A. A. Adcock, G. T. Houlsby, A. G. L. Borthwick, The extractable power from the Pentland Firth, Renewable Energy 63 (2014) 650 – 657.

[13] S. Draper, T. A. A. Adcock, G. T. Houlsby, A. G. L. Borthwick, An Electrical Analogy for the Pentland Firth Tidal Stream Power Resource, Proceedings of the Royal Society A 470 (2014) 20130207.

[14] R. Vennell, Tuning turbines in a tidal channel, J. Fluid Mech. 663 (2010) 253–267.

[15] T. A. A. Adcock, S. Draper, Power extraction from tidal channels – multiple tidal constituents, compound tides and overtides, Renewable Energy 21 (2014) 797 – 806.

[16] G. D. Egbert, R. D. Ray, Semi-diurnal and diurnal tidal dissipation from topex/poseidon altimetry, Geophysical Research Letters 30 (17) (2003) n/a–n/a. doi:10.1029/2003GL017676.
URL http://dx.doi.org/10.1029/2003GL017676

[17] B. B. Parker, A. M. Davies, J. Xing, Tidal height and current prediction, in: C. N. K. Mooers (Ed.), Coastla Ocean Prediction, American Geophysical Union, 1999.

[18] C. Stock-Williams, S. Parkinson, K. Gunn, An investigation of uncertainty in yield prediction for tidal current farms, in: 10th European Wave and Tidal Energy Conference (EWTEC), Aalborg, Denmark, 2013.

[19] S. Muchala, R. H. J. Willden, Impact of support structures on turbine farm power, in: T. Nishino (Ed.), 3rd Oxford Tidal Workshop, Oxford, 7 – 8 April, 2014.

[20] T. A. A. Adcock, On the Garrett and Cummins limit, in: Oxford Tidal Energy Workshop, 29 – 30 March, Oxford, UK, 2012.

[21] R. Vennell, T. A. A. Adcock, Energy storage inherent in large tidal turbine farms, Proceedings of the Royal Society A: Mathematical, Physical and Engineering Science 470 (2166). doi:10.1098/rspa.2013.0580.

[22] C. Garrett, P. Cummins, The power potential of tidal currents in channels, Proceedings of the Royal Society A: Mathematical, Physical and Engineering Science 461 (2060) (2005) 2563–2572. arXiv:http://rspa.royalsocietypublishing.org/content/461/2060/2563.full.pdf+html, doi:10.1098/rspa.2005.1494.
URL http://rspa.royalsocietypublishing.org/content/461/2060/2563.abstract